Published in final edited form as:

Biomacromolecules. 2021 February 08; 22(2): 275–288. doi:10.1021/acs.biomac.0c00947.

Engineering a chemically defined hydrogel bioink for direct bioprinting of microvasculature

Ryan W. Barrs[a,b,‡], **Jia Jia**[a,‡,•], **Michael Ward**[a], **Dylan J. Richards**[a,†], **Hai Yao**[a], **Michael J. Yost**[b,c], **Ying Mei**[a,c,*]

[a]Department of Bioengineering, Clemson University, USA

[b]Department of Surgery, Medical University of South Carolina, USA

[c]Department of Regenerative Medicine and Cell Biology, Medical University of South Carolina, USA

Abstract

Vascularizing printed tissues is a critical challenge in bioprinting. While protein-based hydrogel bioinks have been successfully used to bioprint microvasculature, their compositions are ill-defined and subject to batch variation. Few studies have focused on engineering proangiogenic bioinks with defined properties to direct endogenous microvascular network formation after printing. Here, a peptide-functionalized alginate hydrogel bioink with defined mechanical, rheological, and biochemical properties is developed for direct bioprinting of microvascularized tissues. An integrin-binding peptide (RGD) and a vascular endothelial growth factor (VEGF)-mimetic peptide with a protease-sensitive linker (MMPQK) are conjugated onto biodegradable alginate to synergistically promote vascular morphogenesis and capillary-scale endothelial tube formation. Partial ionic crosslinking before printing converts the otherwise unprintable hydrogel into a viscoelastic bioink with excellent printability and cytocompatibility. We use the bioink to fabricate a compartmentalized vascularized tissue construct, wherein we observe pericyte-endothelial cell colocalization and angiogenic sprouting across a tissue interface, accompanied by deposition of fibronectin and collagen in vascular and tissue components, respectively. This study provides a tunable and translational “off-the-shelf” hydrogel bioink with defined composition for vascularized bioprinting.

Graphical Abstract

[*]**Corresponding Author**: mei@clemson.edu. Phone: 843-876-2548.

[†]**Present Addresses** Immunology Translational Sciences, Janssen Research and Development, LLC, Spring House, PA, USA

[•]School of Life Sciences, Shanghai University, Shanghai 200444, P. R. China

[‡]Author Contributions

These authors contributed equally to this manuscript. All authors have given approval to the final version of the manuscript.

The authors declare no conflict of interest.

Supporting Information

The following files are available free of charge.

- Binarized SEM images, additional rheological measurements, vascular morphogenesis and bioprinting images (PDF)
- Video clip of drop-on-demand bioprinting process (WMV)

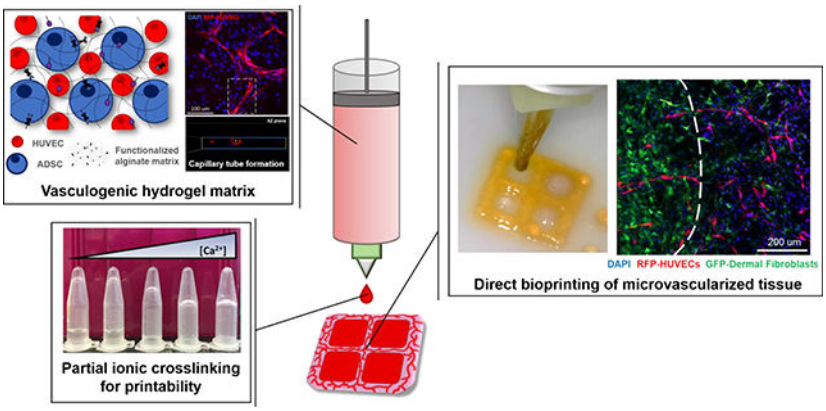

Keywords

alginate; bioink; bioprinting; angiogenesis; vascularization

INTRODUCTION

Three-dimensional bioprinting provides a powerful platform to fabricate prevascularized tissues and organs.[1–4] Microvessels, such as arterioles, venules, and capillaries, primarily regulate local blood-tissue nutrient exchange[5] and play an essential role in supporting the viability of bioprinted constructs.[6] Printable biomaterials, or bioinks, are the “raw materials” of bioprinting and have been used to print microvascular networks through direct and indirect approaches. Significant progress has been made in the past decade to develop sacrificial biomaterials and printing techniques for indirectly patterning vascular networks within bioprinted constructs.[7–9] However, networks made by indirect methods are often >100 microns in diameter, making the approach less suitable for printing complex capillary networks that range from 3 to 10 μm in diameter.[10] Furthermore, the post-printing process associated with removing fugitive materials and endothelializing the hollow networks is complex and time-consuming.[10–13] Direct bioprinting provides a powerful alternative approach to fabricating microvasculature whereby cell-instructive bioinks are used to promote endogenous self-assembly of endothelial cells into capillary networks.[10] However, this approach is currently limited by the low availability of bioinks tailored to promote vasculogenesis while satisfying rheological and printability criteria.[11, 13]

Hydrogels are excellent bioink candidates as they can mimic the biophysical and biochemical properties of the extracellular matrix (ECM).[14–17] Naturally derived hydrogels such as fibrin[18], collagen[19], gelatin[20, 21], and decellularized extracellular matrix (dECM)[22] have been widely used for vascularized bioprinting due to their innate bioactivity. However, the complex matrix characteristics of protein-derived biomaterials complicates fine-tuning of their proangiogenic properties and makes their compositions subject to batch variation.[13, 15, 23–26] Alternatively, synthetic and semisynthetic hydrogels can be chemically modified with bioactive sites like ECM-mimetic peptides, immobilized signaling peptides, and protease-sensitive crosslinkers for defined control over material properties and microengineering of cell-material interactions.[27–30] Alginate, a naturally derived

polysaccharide, is a popular synthetic ECM-mimetic biomaterial used in bioink formulations due to its biocompatibility, low cost, and rapid gelation kinetics.[31, 32] Native alginate is bioinert, but can be modified with cell-adhesive peptides to tailor its bioactivity with excellent precision and control.[33] Furthermore, the biodegradability of alginates can be controlled through partial oxidation of uronic acids in the polymer chain.[34] Various other physical and chemical modifications can be made to fine-tune the chemical and physical properties of alginate hydrogels.[35] These features make alginate an ideal canvas material for developing chemically defined bioinks with requisite printability and cytocompatibility.

Here, we developed an alginate-based hydrogel bioink for the direct fabrication of microvascularized tissue constructs (Figure 1). To promote vascular morphogenesis, the alginate was modified with RGD, an integrin-binding peptide for cell adhesion, and a vascular endothelial growth factor (VEGF) mimetic peptide with a matrix metalloproteinase-cleavable linker (MMPQK) for on-demand sequestration by migratory cells. In a coculture of human umbilical vein endothelial cells (HUVECs) and human adipose derived stem cells (hADSCs), the alginates functionalized with both RGD and MMPQK significantly enhanced vascular morphogenesis at day 7 compared to hydrogels with RGD or MMPQK alone. Importantly, removing soluble VEGF from the culture media did not have a significant effect on the observed vascular morphogenesis in RGD+MMPQK hydrogels, verifying the VEGF-mimetic nature of the MMPQK peptide. Remarkably, lumenized capillary-like networks formed after 14 days of culture without laminar flow. To convert the alginates into a printable bioink, a partial ionic crosslinking approach was employed, and the rheological and printability properties of the partially crosslinked hydrogels were evaluated. As a proof-of-concept, the bioink was applied to fabricate a compartmentalized vascularized tissue unit (VTU), which contained a vascular component (bioink with HUVECs and hADSCs) surrounding avascular tissue components (bioink with human dermal fibroblasts).

EXPERIMENTAL SECTION

Materials.

Sodium alginate was purchased from FMC BioPolymer (Philadelphia, PA). Amino acids and resins were purchased from Protein Technologies, Inc. (Tucson, AZ). Ethylene glycol was purchased from Fisher Scientific (Hamtpon, NH). Hexafluorophosphate Benzotriazole Tetramethyl Uronium (HBTU) was purchased from Oakwood Chemical (Estill, SC). All other materials were purchased from Sigma-Aldrich (St. Louis, MO) unless stated otherwise.

Oxidized alginate preparation.

Oxidized alginate was prepared as described by Bouhadir and others.[34] One gram of sodium alginate powder was dissolved in 100 mL of distilled, deionized water. Sodium periodate was added at room temperature to achieve a theoretical oxidation of 1% of uronic acid units. The solution was stirred in the dark for 24 hours before being terminated with addition of ethylene glycol. Sodium chloride (3g) was then dissolved in the solution. Oxidized alginate was precipitated with addition of excess ethyl alcohol and centrifuged into a pellet. The

supernatant was discarded, and the precipitation was repeated. The oxidized alginate pellets were frozen at −80°C overnight then lyophilized and stored at −20°C until use.

Peptide synthesis and conjugation to oxidized alginate.

Alkynyl-modified RGD peptides (Alkynyl-modified G_4RGDSP, M.W. = 895.89 kDa, MOLDI-TOF = 896.33 kDa) and Alkynyl-modified MMPQK peptides (Alkynyl-modified GPQGIAGKLTWQELYQLKYKGI, M.W. = 2628.04 kDa, half peak = 1315.00 kDa) were synthesized through solid phase peptide synthesis (SPPS), purified through flash column, and synthesis verified through liquid chromatography–mass spectrometry (LC-MS) on a Thermo Fisher LCQ Fleet Ion Trap Mass Spectrometer. Later, the peptides were covalently conjugated to oxidized alginate using orthogonal “click” chemistry. The degree of peptide functionalization was examined by ^{1}H-NMR on Bruker AV500-III spectrometers. The characteristic peak of the proton on alginate backbone and the proton on the triazole were compared to determine the degree of peptide conjugation. Peptide conjugation to alginate at 0.135 mmol/g (peptide/alginate powder) for RGDSP and 0.148 mmol/g (peptide/alginate powder) for MMPQK were utilized for the rest of the experiments unless otherwise stated.

Preparation of alkynyl-functionalized peptides.

The peptides were prepared SPPS conducted using the standard procedure described in the Novabiochem peptide synthesis manual. N-terminal unmodified peptides were cleaved from resin right after the deprotection once reaching the designed sequences. Alkynyl functionalization of peptides was carried out similarly to Zhang and Killian [36]. Briefly, the mixture of 1-ethyl-3-(3-dimethylaminopropyl)carbodiimide (EDC) (0.3 mmol), N-hydroxysuccinimide (NHS) (0.3 mmol) and 4-Oxo-4-(2-propynyloxy)butanoic acid (Matrix Scientific, Columbia, SC) (0.3 mmol dissolved in DMF) was used to form the active NHS ester to react with the terminal amine group of the peptide chain (0.1 mmol) before they were cleaved from the resin. All the peptides were purified by flash column and characterized by LC-MS.

Preparation of azide-functionalized alginate.

198 mg of oxidized alginate was dissolved in 50 mL DI water. The mixture of EDC (19.2 mg), NHS (11.5 mg) and 11-Azido-3,6,9-trioxaundecan-1-amine (21.8 mg) was added into the alginate solution and the reaction was performed for 24 hours. After that, the alginate was purified through ethanol precipitation. The alginate powder was obtained through lyophilization for later usage.

Conjugation of alkynyl-functionalized peptides onto alginate.

Copper(I)-assisted alkyne-azide cycloaddition (CuAAC) “click” chemistry was conducted as follows. 198 mg of azide-functionalized alginate was dissolved in 50 mL DI water. The mixture of $CuSO_4$ (16 mg), ascorbic acid (88 mg), Tris(3-hydroxypropyltriazolylmethyl)amine (THPTA) (265 mg) and peptides (0.1 mmol) was added into the alginate solution and the reaction was performed for 24 hours. After that, the alginate was purified through ethanol precipitation and alginate powder was obtained through lyophilization for later usage.

Hydrogel preparation and SEM analysis.

Functionalized alginate hydrogels were prepared for scanning electron microscopy (SEM) imaging through freeze drying, as described previously.[37] Briefly, 60 μL of peptide-functionalized, 2% (w/v) alginate solution was pipetted onto 100 mM Ca^{2+}-containing gelatin substrates in a 24-well plate for crosslinking overnight at 4 °C. The calcium-gelatin substrate was then melted in a 37 °C incubator for 15 minutes before being aspirated, and the hydrogels were then frozen at −20 °C for 3 hours, followed by −80 °C for 24 hours, and then lyophilized for at least 24 hours. The freeze-dried hydrogels were then gold sputter-coated at 20 milliamps for 20 seconds (Denton Vacuum Desk V) and microstructures were observed in a scanning electron microscope (Hitachi S-3700N). SEM images at 200x magnification were analyzed using ImageJ software[38] with the DiameterJ plugin[39]. The percentage of porosity of the hydrogels was quantified from three independent regions of interest in each of three individual hydrogels. First, the images were binarized using a statistical region-merging algorithm[40], then the percentage of porosity was calculated from the areas of black (pores) and white (scaffold) pixels within the binary images.

Cell culture.

RFP expressing human umbilical vein endothelial cells (RFP-HUVECs) (Angio-Proteomie, Boston, MA) were maintained in complete Endothelial Cell Growth Medium 2 (EGM-2) (PromoCell, Heidelberg, Germany) with 10% (v/v) Fetal Bovine Serum (FBS) and 1% Penicillin-Streptomycin. hADSCs (Lonza, Walkersville, MD) were maintained in complete ADSC Growth Medium (ADSCGM) (Lonza) with 10% (v/v) FBS and 1% gentamicin sulfate. GFP expressing adult human dermal fibroblasts (GFP-hDFs) (Angio-Proteomie) were maintained in complete Fibroblast Growth Medium 2 (FGM-2) (PromoCell) with 2% FBS. All cells used were between passages 3–6.

Hydrogel cell behavior studies and image analysis.

Oxidized alginates functionalized with either RGD only, MMPQK only, or both RGD and MMPQK were dissolved in culture medium (2:1 EGM-2:ADSCGM) at a concentration of 2% (w/v) alginate. Peptide concentration was 5% (w/w) of the alginate for each peptide. RFP-HUVECs were either suspended alone or with hADSCs at a 2:1 ratio for a total cell density of 5 million cells/mL in each alginate solution. Alginate solutions were pipetted as hydrogel “dots” into the wells of a 96-well plate containing calcium-gelatin substrate for 30 minutes to allow for complete gelation. The plate was then placed in the incubator for 15 minutes to melt the gelatin substrate. The melted substrate was aspirated, the hydrogel was rinsed with PBS, and fresh medium was added to the wells before returning the plate to the incubator. Media was changed every 2–3 days until the hydrogels were taken for imaging. For imaging, the hydrogels were placed onto glass slides in PBS to stay hydrated and RFP-HUVEC morphology was analyzed using a Leica TCS SP5 Confocal microscope or a Zeiss Axiovert A1 Inverted Microscope and Zen 2011 software (Zeiss). Three hydrogel replicates per group were imaged at random and processed with AngioTool[41] as described in their online manual to quantify vessel percentage area, average vessel length, and junction density. For analyzing invasion depth in the Vascularized Tissue Unit after 7 days, sprouting microvascular networks at the tissue bud interface were imaged using confocal microscopy.

A Zeiss Axiovert A1 Inverted Microscope and Zen 2011 software (Zeiss) was used to image vascular invasion at Day 14. The lengths of at least 3 sprouting networks were measured in 3 separate VTUs at Day 7 or 14 using ImageJ. For CD31 and NG2 cell imaging, structures were fixed and stained with anti-CD31 (BD Pharmingen, 550389) and anti-NG2 antibody (Abcam, ab129051) following the manufacturer's protocol and imaged via confocal microscopy. For ECM staining, the samples were fixed and stained with anti-fibronectin (Abcam, ab45688) or anti-collagen I antibody (Abcam, ab34710) following the manufacture's protocol and imaged via confocal microscopy. The relative quantities of secreted fibronectin and collagen were quantified and compared by measuring background-subtracted integrated density ($n \geq 4$) in the vascular and tissue components, respectively.

Partial crosslinking of alginate.

To prepare partially crosslinked alginates, stock solutions of calcium chloride dihydrate dissolved in water were prepared at concentrations of 0, 5, 10, and 20, and 30 mM. The stock solutions were slowly added to a 4% (w/v) alginate solution at a volume ratio of 1:1, yielding 2% (w/v) alginate solutions containing 0, 5, 10, and 15 mM $CaCl_2$. The solutions were vortexed for one minute and left in the refrigerator overnight to ensure homogenous mixing.

Rheological studies.

Rheological measurements were performed using an AR-G2 rheometer (TA Instruments). For characterization of peptide-functionalized hydrogels, an 8 mm standard steel parallel plate geometry with a measurement gap of 1 mm was used. A dynamic oscillatory frequency sweep from 0.5 to 100 rad/s at 1% strain was used to compare storage and loss modulus between hydrogel groups. A solvent trap was used to keep gels hydrated during testing. For characterization of partially crosslinked RGD and MMPQK-functionalized alginate precursors, a 25 mm standard steel parallel plate geometry with a measurement gap of 500 μm was used. A shear rate ramp from 0.001 to 1000 (1/s) was used to evaluate the flow of the solutions and find yield stress. A dynamic oscillatory frequency sweep from 0.1 to 10 Hz at 1% strain was used to measure storage and loss modulus. All measurements were taken at room temperature and a two-minute equilibration step was performed before each run.

Printability studies.

The capability of partially crosslinked alginate to successfully print a computer-designed lattice structure was evaluated using a point-to-point fabrication method (detailed next section). Alginate solutions were dyed with red food coloring for visualization. Cell sedimentation in the partially crosslinked alginate was evaluated using glass pipette tips with an agarose plug at the end. HUVECs and hADSCs were stained with Calcein-AM before being suspended 2:1 in partially crosslinked alginate at a total density of 3 million cells/mL and pipetted into the glass tips. The tips were left upright at room temperature for 3 hours before being visualized with fluorescent microscopy. Cell viability was assessed in hydrogels immediately post-printing using a LIVE/DEAD cell viability assay according to the manufacturer's instructions (Cat.# L3224, Thermofisher). To evaluate bioprinting consistency, lattice structures were sequentially bioprinted ($n = 4$) with 15 mM partially crosslinked bioink and the images of the structures were captured. The length (x-axis) and

width (y-axis) at three different sections of each construct, as well as pore diameter, were measured and compared among all the constructs to determine the repeatability and consistency of printing using the partially crosslinked bioink. To evaluate printing accuracy compared to a CAD model, a lattice structure was designed through Visual PathBuilder software (Ratioserv). The printing was performed to fabricate the structures based on the CAD design and after printing, the length (x-axis), width (y-axis) and pore diameter of the printed structures were measured (n≥3) and compared to the original CAD design to determine the relative percent accuracy according to the following equation: Percent accuracy = 1- $|(D_{CAD}-D_{print})/D_{CAD}|\cdot 100\%$, where D_{CAD} and D_{print} are the dimensions of the CAD-designed construct and actual printed construct, respectively.

Bioprinting process.

All bioprinting in this study was performed on the Palmetto Printer - a fully automated, piston-driven bioprinter at the Medical University of South Carolina. The Palmetto Printer has three interchangeable dispensers, a temperature-controlled printing surface, and HEPA filtration system. The bioprinter was sealed under positive pressure and sterilized with UV light for at least 10 minutes before printing syringes were loaded. To fabricate a vascularized tissue unit, two dispensers were used – one containing our vasculogenic bioink (vascular component) and the other a fibroblast-containing bioink (tissue component). The vasculogenic bioink contained alginate functionalized with 5% (w/w) RGD and MMPQK peptides. The fibroblast-containing bioink was alginate functionalized with 5% (w/w) RGD only. The bioinks were dissolved in cell culture media at 2% (w/v) concentration and partially crosslinked as described in a previous section. To fabricate a heterogenous VTU, RFP-HUVECs and hADSCs were suspended in the vasculogenic bioink in a 2:1 ratio (RFP-HUVEC:ADSC) at a total cell density of 5 million cells/mL. To fabricate a mixed VTU, RFP-HUVECs, hADSCs, and GFP-hDFs were suspended in the vasculogenic bioink in a 2:1:1 ratio (RFP-HUVEC:ADSC:GFP-hDF) at a total cell density of 5 million cells/mL. For both heterogenous and mixed VTUs, GFP-hDFs were loaded at a density of 2 million cells/mL in the fibroblast-containing bioink. The cell-laden bioinks were loaded into sterile, printer-compatible syringes with 20 ga. dispensing tips before being transported to the bioprinter. Printing speed was 10 μL/sec and droplet volume was 230 nL A $CaCl_2$-containing substrate was maintained at 4°C on the printing plate to prevent the gelatin from melting. A point-to-point method was used to print the Vascularized Tissue Unit construct. First, the vasculogenic bioink was printed into a single-layer lattice construct by depositing an outline of dots separated by 600 μm and then printing dots between the gaps of the outline, allowing the dots to combine and make a cohesive structure. Fibroblasts were then printed into the voids of the lattice with a second dispenser to form the tissue component (~1.2 mm diameter). After printing was completed, the constructs were left to fully crosslink on the $CaCl_2$-containing substrate for 15 minutes. Then, 4 mL of culture media was added, and the petri dish was incubated at 37°C for 10 minutes to allow the gelatin substrate to melt. The constructs were removed from the dish and individually placed into wells of a 12-well plate. The constructs were cultured in media containing 50% EGM-2, 25% ADSC-GM, 25% FGM-2, and 1% Penicillin Streptomycin (Pen Strep). Media was changed every other day.

$CaCl_2$-containing gelatin substrate preparation for bioprinting.

Porcine gelatin (3% wt.), sodium chloride (0.9% wt.), calcium chloride (100 mM), and titanium dioxide (2% wt.) were added to distilled, deionized water, and boiled to dissolve the gelatin. For cell behavior studies, the substrate was distributed into the wells of a 96-well plate. For bioprinting, 5 mL aliquots were pipetted into standard petri dishes and left to solidify overnight at 4°C. Addition of titanium dioxide increased the substrate's opacity so that position sensing lasers on the bioprinter could detect the printing surface.

Statistical analysis.

All variables were expressed as means ± standard deviations (S.D.). One-way ANOVA with Tukey's multiple comparisons test was used to compare percent porosity of functionalized alginate hydrogels, vascular morphogenesis parameters between RGD+MMPQK, RGD only, and MMPQK only hydrogels, yield stress and zero shear viscosity among partially crosslinked alginate solutions, and construct dimensions among sequentially printed lattices. A Student's *t*-test was used to compare vascular morphogenesis with or without VEGF, angiogenic sprouting from the strut and junction regions in the printed VTU, and ECM deposition in the vascular and tissue components. Two-way ANOVA with Tukey's multiple comparisons test was used to compare storage and loss modulus among peptide-functionalized alginates. For all analyses, a value of $p < 0.05$ was considered statistically significant.

RESULTS AND DISCUSSION

Vasculogenic hydrogel matrix design and synthesis.

Native alginate is bioinert and non-degradable. In our previous work, we developed strategies to engineer alginate as a cytocompatible, biodegradable bioink through cell-adhesive peptide modification and partial oxidization.[42] To ensure a high conjugation efficiency between the alginate and peptides, we utilized CuAAC "click" chemistry-mediated bioconjugation in this study (Figure 1A).

In addition to RGDSP, which targets multiple integrins (e.g. $\alpha_v\beta_3$) involved in angiogenesis and vascular development[43], MMPQK peptides were used to further promote vascular morphogenesis[44–47] through cell-demanded release from the alginate matrix and binding of VEGF receptors[48–52] (Figure 1B, C). The inclusion of MMPQK was intended to mimic the sequestration of matrix-bound VEGF via MMPs released from migratory endothelial cells, which is essential for vascular patterning.[53, 54] Together, these two peptide ligands were selected for vasculogenic bioink development as the cross-activation between integrins (i.e. $\alpha_v\beta_3$) and VEGF receptors in endothelial cells has been reported to synergistically induce angiogenic signaling.[55–57]

Chemical and physical characterization of peptide-functionalized alginate hydrogels.

The success of conjugation between alginates and peptides was monitored by LC-MS. Notably, there was no detectable peptide in the liquid residual after reaction, indicating the completion of the conjugating reaction (Figure 2A). We further validated the degree of peptide functionalization using ^{1}H-NMR (Figure S1, Supporting Information), and found

that RGD and MMPQK peptides were successfully conjugated to alginate at 0.135 mmol/g (peptide/alginate powder) and 0.148 mmol/g, respectively. As mechanical properties (e.g., elasticity) of hydrogels have been shown to significantly affect vascular morphogenesis[58, 59], we examined the storage and loss modulus of 2% (w/v) peptide-functionalized alginates. We found similar values across all conditions (Figure 2B), indicating the similar physical macro-environment of these hydrogels. Further, the microstructures of the peptide-functionalized alginate hydrogels showed similar pore structures and porosity percentage values (Figure 2C) as calculated from binarized SEM images (Figure S2, Supporting Information). Together, these data indicated that peptides were successfully conjugated to the alginate matrices and that the hydrogels had similar mechanical and microstructural properties, providing a controlled environment to study peptide effects on vascular morphology in subsequent analyses.

Vascular morphogenesis in functionalized alginate hydrogels.

To examine the effects of RGD and MMPQK peptides on microvascular network formation, RFP-expressing HUVECs and hADSCs were encapsulated in 2% (w/v) peptide-functionalized alginate hydrogels and cultured for 7 days. Vascular morphogenesis was quantified by HUVEC fractional area, average vessels length, and junctions/mm^2 (Figure 3A, B). All three metrics were significantly improved in the hydrogels functionalized with both RGD and MMPQK peptides compared to hydrogels functionalized with either peptide alone. These results support previous findings that coactivation of integrins and VEGF receptors results in synergistic signaling that enhances vascular morphogenesis.[55, 60–62] To study the potential vasculogenic effects of soluble VEGF[63] in the culture media, we removed the VEGF supplement from the media. We found that removing VEGF from the media led to insignificant changes in vascular morphogenesis in the RGD+MMPQK hydrogels (Figure 3C, D). This suggests that the observed vascular network formation did not rely on the soluble VEGF present in the culture media.

Importantly, coculture with hADSCs was required for the formation of endothelial cord-like networks (Figure 3A). Without hADSCs, vascular morphogenesis was severely limited and HUVECs retained a round morphology after 7 days. These results agreed with previously observed cooperation between hADSCs and endothelial cells during vasculogenesis.[64, 65] Colocalization of HUVECs and hADSCs was observed at day 7 in co-culture (Figure S3, Supporting Information), further indicating that hADSCs directly interacted with microvascular networks.

To analyze the maturation of microvascular networks formed in the 2% (w/v) RGD +MMPQK functionalized alginate hydrogels, we extended the culture period. At day 14, extensive microvascularization was observed within the hydrogels and HUVECs had assembled into lumenized networks (Figure 3E). This was a significant observation given the defined composition of the hydrogels and the static culture conditions. Hollow lumens were found within these networks as evidenced by 3D reconstruction and, notably, the lumens had a diameter of approximately 9 μm (Figure 3F), which falls within the range of capillaries.[66] While some laser-based bioprinting techniques can fabricate channels of this scale, endogenous capillary network formation facilitated by vasculogenic biomaterials is a more

facile, biomimetic approach for direct capillarization. We reason that in our alginate matrix, HUVECs form lumenized networks by simultaneously binding to RGD peptides via $\alpha_v\beta_3$ integrins, and proteolytically demanding the release of MMPQK peptides throughout migration as the hydrogel degrades through hydrolysis during culture. Interestingly, previous literature has also highlighted similar required factors (integrin and VEGFR activation) for vascular network formation in an engineered MMP-labile crosslinker composed hyaluronic acid matrix.[67]

Processing peptide-functionalized hydrogel precursors into a viscoelastic bioink via partial crosslinking.

The rheological properties of a bioink are directly correlated with its printability.[17, 68–73] The 2% (w/v) alginate solution was initially not suitable for high fidelity bioprinting because of its low viscosity (<1 Pa·s).[42] Increasing the polymer concentration to raise the viscosity was not appropriate as a concentration of only 4% (w/v) alginate inhibited network formation (Figure S4, Supporting Information) and was still not viscous enough to print. To improve the printability of the low-concentration alginate bioink, we employed a partial ionic crosslinking approach to increase the viscosity of the alginate solutions. Gradually adding aqueous calcium chloride ($CaCl_2$) to 4% (w/v) peptide-functionalized alginate at a 1:1 (v/v) ratio progressively crosslinked the alginate hydrogel precursor into a more viscous solution, but not a fully solidified hydrogel (Figure 4A).

We then used the partial crosslinking strategy to modify the rheological properties of the peptide-functionalized alginate solutions, as these attributes (i.e. yield stress, shear thinning, viscoelasticity) directly influence printability.[73–75] Alginate solutions containing 0 mM or 5 mM $CaCl_2$ exhibited exceptionally low yield stress (<0.01 Pa) while the 10 mM and 15 mM $CaCl_2$ crosslinked solutions exhibited non-linear pseudoplastic fluid behavior with significantly higher yield stresses (Figure 4B, C). Since alginate exhibits non-Newtonian fluid behavior, the Herschel-Bulkley model was used to calculate the yield stress of partially crosslinked alginate solutions[76] (Figure S5, Supporting Information). The 10 mM solution had a yield stress of 1.7 ± 0.3 Pa, while the 15 mM solution was significantly higher at 5.3 ± 0.3 Pa (Figure 4C). The viscosity of the 15 mM solutions declined rapidly in a shear rate sweep, exhibiting highly shear thinning behavior (Figure 4D). Based on the Cross model[77], the zero shear viscosity of the 15 mM solution (471.8 ± 43.73 Pa.s) was over an order of magnitude greater than that of the 10 mM solution (15.63 ± 9.75 Pa.s) and more than two orders of magnitude greater than that of the 0 and 5 mM solutions (both <1 Pa.s) (Figure 4E and Figure S6, Supporting Information). Therefore, the viscosity of the 15 mM solution was most suitable for bioprinting. The 15 mM $CaCl_2$ solution demonstrated stable viscoelastic properties, as the storage modulus (G') was larger than the loss modulus (G") during a frequency sweep from 0.1 to 10 Hz (Figure 4F). The 20 mM $CaCl_2$ crosslinked alginate was not evaluated as it could not be loaded into a printing syringe due to complete gelation and, therefore, would be incompatible with bioprinting. By partially crosslinking the alginate hydrogel precursor with an optimal concentration of crosslinker before printing, we were able to meet several major rheological criteria for printable bioinks without increasing polymer concentration. Through the above optimization, we successfully formulated alginate into a viscoelastic fluid which meets several major rheological criteria for printable

bioinks without increasing polymer concentration. These results agree with previous reports that have used partial crosslinking to improve the printability of low-concentration alginate bioinks for tissue engineering.[23, 78] However, we have reformed this strategy to improve the printability of a proangiogenic hydrogel bioink for direct vascularized bioprinting.

Printability of the partially crosslinked vasculogenic hydrogel bioink.

Since the 2% (w/v) vasculogenic alginate solution partially crosslinked with 15 mM $CaCl_2$ was the most suitable candidate for bioprinting, we next evaluated its printability according to several benchmarks. Since bioprinting complex tissues and organs may require hours-long printing times, we firstly performed a sedimentation test with HUVECs and hADSCs to evaluate the ability of the bioink candidate to keep these cells homogenously suspended for a prolonged printing time (3 hours). Most of the cells in the non-partially crosslinked alginate sank to the bottom of the reservoir after 3 hours, while cells remained homogenously suspended in the partially crosslinked alginate (15 mM $CaCl_2$) (Figure 5A). This demonstrated the capacity of the bioink to prevent sedimentation of encapsulated cells over a 3-hour printing period, which is important since sedimentation during printing would result in inhomogeneous cell deposition in the final construct. Importantly, most of the cells were still viable after 3 hours, as indicated by the live-cell Calcein-AM staining used to label the cells in the reservoir.

When utilized to print a lattice structure in a drop-on-demand approach (Video S1, Supporting Information), the partially crosslinked alginate (15 mM $CaCl_2$) successfully printed a cohesive lattice, whereas a disconnected lattice was printed when using the non-partially crosslinked alginate (Figure 5B), which could be attributed to partially crosslinked strategy significantly improving printing resolution (Figure 5C). A homogenous distribution of cells was observed in the printed lattice structure using partially crosslinked alginate (15 mM $CaCl_2$) (Figure S7, Supporting Information), consistent with the results of the sedimentation test. We further evaluated the printing consistency and accuracy of the partially crosslinked bioink by sequentially printing lattice constructs and comparing their dimensions amongst themselves as well as to the original CAD design. The mean print accuracy was >90% for all construct dimensions (i.e. length, width, and pore size) compared to the original CAD design (Figure 5D) and there was no significant difference in construct dimensions among sequentially printed constructs (Figure 5E). Therefore, the partially crosslinked bioink printed constructs with excellent repeatability and accuracy. In addition, most cells (>90%) remained viable after printing (Figure 5F). This could be attributed to the shear thinning properties of alginate-based hydrogels[79], wherein the physically crosslinked matrix undergoes a reversible gel-sol transition during extrusion, shielding suspended cells from shear stresses at the nozzle orifice.[80]

Combined with the outcomes of rheological tests, these results demonstrated that partially crosslinking alginate hydrogel precursor provides an effective strategy to process low-viscosity vasculogenic hydrogels into printable bioinks for bioprinting microvascularized tissues.

Fabricating heterogenous vascularized tissue with the vasculogenic bioink.

To validate the capacity of our bioink for direct printing of microvascularized tissues, we fabricated a VTU, which is a heterogenous soft tissue construct composed of vascular and tissue-specific components to mimic stromal and parenchymal elements of soft tissues.[81, 82] Using a multi-nozzle bioprinter, the vascular component was printed first with our vasculogenic bioink in a lattice structure. A second nozzle was then used to print tissue-specific “buds” within the voids of the lattice. For the tissue component, we used an RGD-functionalized bioink containing GFP-hDFs (Figure 6A). Dermal fibroblasts were used as a proof-of-concept for the tissue component as they maintain the ECM in the dermis layer of the skin and modulate wound healing.[83]

After printing, the vascular and tissue components could be distinguished in a cohesive structure under bright-field microscopy and cells appeared homogenously distributed in both components (Figure 6B). After 7 days in culture, the vascular component contained extensive microvascular networks in the strut and junction regions that sprouted into the tissue component (Figure 6C, D). Importantly, the RGD+MMQPK bioink promoted greater CD31+ fractional area coverage and average vessels length by RFP-HUVECs within the vascular component compared to the RGD only bioink (Figure S8, Supporting Information), indicating that the RGD+MMPQK bioink significantly promotes a vascular-specific phenotype and function of endothelial cells compared to RGD-functionalized alginate, which is a state-of-the-art peptide-functionalized alginate bioink for vascularized bioprinting. The average invasion depth of microvasculature from the vascular component (either from the junction part of the structure or from the strut part of the structure) into the tissue component was around 200 μm at day 7 (Figure S9, Supporting Information). Interestingly, NG2+ mural cells were found tightly colocalized with RFP-HUVECs in the vascular component, indicating a pericyte-like functional role of hADSCs for vascular development in the construct, consistent with previous literature[84, 85] (Figure 6E).

After extended culture for 14 days, average invasion depth from the vascular component into the tissue component had tripled to around 650 μm (Figure S10, Supporting Information). Remarkably, vascular invasion into the tissue component was only observed in a heterogenous VTU construct, wherein dermal fibroblasts were printed only in the tissue component and not in the vascular component. When dermal fibroblasts were printed in the vascular component along with RFP-HUVECs and hADSCs (“mixed” VTU), we observed no invasion into the tissue component (Figure S10, Supporting Information). This validated the biomimetic design of the VTU with compartmentalized vascular components and tissue components. This is also in agreement with a recent study that demonstrated enhanced vascularization in a heterogenous, compartmentalized muscle tissue construct compared to a homogenous, mixed construct.[22] These results show that the RGD+MMPQK bioink can effectively promote vascular network invasion at a heterogenous tissue interface.

Additionally, we observed endogenous deposition of fibronectin, a key ECM protein involved in blood vessel formation[86, 87], in the vascular component of the VTU (Figure 7A). Compared to the tissue component, there was significantly greater fibronectin deposition in the vascular component (Figure 7B), indicating promotion of vascular-specific matrix assembly by the RGD and MMPQK peptides. Compared to the deposition of fibronectin in

the vascular component, significantly more type I collagen was observed in tissue components, indicating normal function of fibroblasts (Figure S11, Supporting Information).

Collectively, these results not only provided in situ evidence of the ability of our bioink to support vascular morphogenesis, but they also demonstrate the feasibility of designing peptide-functionalized bioinks for direct fabrication of heterogenous microvascularized tissue components. The bioink developed in this study could be applied in other multi-material or multi-nozzle techniques to print a variety of complex vascularized tissue-specific constructs. The presently described VTU could have immediate applications in wound healing or as a modular in vitro vascularized test bed for drug toxicity assays.[88] However, the bioink used to print the tissue component of the VTU needs to be further optimized to accelerate vascular invasion from the vascular component, as portions of the tissue component were still not vascularized at Days 7 and 14. Future studies could also explore the feasibility of fabricating VTUs containing other parenchymal cell types in the tissue component (ex. cardiomyocytes, hepatocytes, neurons, etc.) for vascularized organ-on-chip models. For example, Hooper and others proposed using vascular-specific and neural-specific hydrogel bioinks to fabricate a neurovascular unit (NVU) that could be used to study neurovascular function and dysfunction in vitro.[89] The modularity of the VTU makes it a conceivable platform for bottom-up manufacturing of vascularized soft tissues for various tissue engineering applications, though in vivo studies are necessary to determine the capacity of the VTU to anastomose with host vasculature.

CONCLUSIONS

In summary, a vasculogenic alginate hydrogel bioink with defined chemistry was developed to recapitulate functional cues of the natural ECM and promote microvascular network formation in bioprinted tissue constructs. Chemical modification with RGDSP and MMPQK peptides provided a defined, tunable matrix for directly promoting endogenous microvascularization and established a foundational biomaterial for subsequent processing into an animal origin-free bioink engineered for bioprinting microvasculature.

While the hydrogel precursor was initially not printable, converting the low-viscosity solution into a printable bioink was accomplished with a partial crosslinking strategy, avoiding the need to increase polymer concentration, which would impede vascular morphogenesis. Furthermore, this strategy circumvented the need for blending with chemically undefined biomaterials like gelatin or collagen, preserving the defined chemical nature of our bioink matrix. By thoroughly characterizing rheological properties governing bioprintability, we demonstrated that partial crosslinking of alginate hydrogels is a facile approach to significantly improving the printability of low viscosity alginate bioinks. While bio-inert partially crosslinked alginate has been used previously by Tabriz and others to print alginate hydrogel structures with cells to demonstrate biocompatibility of the partial crosslinking strategy[78], this is, to the best of our knowledge, the first time partial crosslinking has been employed to develop a bioactive, peptide-functionalized alginate hydrogel bioink for printing heterogenous, vascularized soft tissue while satisfying rheological and printability for bioprinting. Our bioink would be amenable to other robotic dispensing methods, such as freeform reversible embedding of suspended hydrogels

(FRESH)[90] and coaxial extrusion for 3D fabrication of vascularized tissues. Furthermore, our bioink could complement sacrificial bioprinting approaches to promote direct capillarization of constructs with larger, perfusable macrovasculature.

Future work will seek to optimize the tissue-specific bioink formulation, design of the VTU, and bioprinting technique to achieve complete prevascularization of the bioprinted constructs. These studies could also focus on using other peptides targeting multiple types of integrin/growth factor receptors or combinatorial crosslinking strategies (e.g. physical and chemical crosslinking strategies) to further tune the bioactivities of the alginate and reinforce its mechanical properties, respectively. It is also feasible to design and fabricate VTUs containing other tissue-specific cell types (e.g. cardiomyocytes, hepatocytes, neurons, etc.) to recapitulate heterogenous vascularized tissue/organ components (e.g. heart, liver, brain, etc.). The bioink developed here expands the availability of printable, chemically defined proangiogenic bioink alternatives to protein-based hydrogels like collagen, gelatin, Matrigel, etc. for vascularized bioprinting. The defined nature of the reported vasculogenic bioink matrix makes it a promising, translational “off-the-shelf” bioink platform for robust fabrication of microvasculature and direct microvascularization of bioprinted tissues.

Supplementary Material

Refer to Web version on PubMed Central for supplementary material.

ACKNOWLEDGEMENTS

The authors would like to thank Sarah Grace Dennis Little for helping operate the bioprinter, Peng Chen for helping with rheological characterization, and Aarti Shenoy for assistance with SEM imaging and analysis.

Funding Sources

This work was supported in part by the South Carolina Research Alliance (SCRA) grant “South Carolina National Resource Center in Biomanufacturing”. It was also supported in part by the National Science Foundation EPSCoR Program under NSF Award # OIA-1655740 and the National Institutes of Health (R01 HL133308, 8P20 GM103444). Any opinions, findings and conclusions or recommendations expressed in this material are those of the author(s) and do not necessarily reflect those of the National Science Foundation.

REFERENCES

1. Richards D; Jia J; Yost M; Markwald R; Mei Y, 3D Bioprinting for Vascularized Tissue Fabrication. Ann. Biomed. Eng 2017, 45, (1), 132–147. [PubMed: 27230253]
2. Datta P; Ayan B; Ozbolat IT, Bioprinting for vascular and vascularized tissue biofabrication. Acta Biomater. 2017, 51, 1–20. [PubMed: 28087487]
3. Ozbolat IT, Bioprinting scale-up tissue and organ constructs for transplantation. Trends Biotechnol. 2015, 33, (7), 395–400. [PubMed: 25978871]
4. Murphy SV; Atala A, 3D bioprinting of tissues and organs. Nat. Biotechnol 2014, 32, (8), 773–85. [PubMed: 25093879]
5. Segal SS, Regulation of blood flow in the microcirculation. Microcirculation 2005, 12, (1), 33–45. [PubMed: 15804972]
6. Visconti RP; Kasyanov V; Gentile C; Zhang J; Markwald RR; Mironov V, Towards organ printing: engineering an intra-organ branched vascular tree. Expert Opin. Biol. Ther 2010, 10, (3), 409–20. [PubMed: 20132061]
7. Wu W; DeConinck A; Lewis JA, Omnidirectional Printing of 3D Microvascular Networks. Adv. Mater 2011, 23, (24), H178–H183. [PubMed: 21438034]

8. Miller JS; Stevens KR; Yang MT; Baker BM; Nguyen DH; Cohen DM; Toro E; Chen AA; Galie PA; Yu X; Chaturvedi R; Bhatia SN; Chen CS, Rapid casting of patterned vascular networks for perfusable engineered three-dimensional tissues. Nat. Mat 2012, 11, (9), 768–74.
9. Kolesky DB; Homan KA; Skylar-Scott MA; Lewis JA, Three-dimensional bioprinting of thick vascularized tissues. Proc. Natl. Acad. Sci. USA 2016, 113, (12), 3179–84. [PubMed: 26951646]
10. Ke D; Murphy SV, Current Challenges of Bioprinted Tissues Toward Clinical Translation. Tissue Eng., Part B 2019, 25, (1), 1–13.
11. Gungor-Ozkerim PS; Inci I; Zhang YS; Khademhosseini A; Dokmeci MR, Bioinks for 3D bioprinting: an overview. Biomater. Sci 2018, 6, (5), 915–946. [PubMed: 29492503]
12. Ouyang L; Armstrong JPK; Chen Q; Lin Y; Stevens MM, Void-Free 3D Bioprinting for In Situ Endothelialization and Microfluidic Perfusion. Adv. Funct. Mater 2020, 30, (1), 1908349. [PubMed: 33071714]
13. Barrs RW; Jia J; Silver SE; Yost M; Mei Y, Biomaterials for Bioprinting Microvasculature. Chem Rev 2020, 120, (19), 10887–10949. [PubMed: 32867470]
14. Drury JL; Mooney DJ, Hydrogels for tissue engineering: scaffold design variables and applications. Biomaterials 2003, 24, (24), 4337–51. [PubMed: 12922147]
15. Lutolf MP; Hubbell JA, Synthetic biomaterials as instructive extracellular microenvironments for morphogenesis in tissue engineering. Nat. Biotechnol 2005, 23, (1), 47–55. [PubMed: 15637621]
16. Brandl F; Sommer F; Goepferich A, Rational design of hydrogels for tissue engineering: impact of physical factors on cell behavior. Biomaterials 2007, 28, (2), 134–46. [PubMed: 17011028]
17. Malda J; Visser J; Melchels FP; Jungst T; Hennink WE; Dhert WJ; Groll J; Hutmacher DW, 25th anniversary article: Engineering hydrogels for biofabrication. Adv. Mater 2013, 25, (36), 5011–28. [PubMed: 24038336]
18. Cui X; Boland T, Human microvasculature fabrication using thermal inkjet printing technology. Biomaterials 2009, 30, (31), 6221–7. [PubMed: 19695697]
19. Lee VK; Lanzi AM; Haygan N; Yoo SS; Vincent PA; Dai G, Generation of Multi-Scale Vascular Network System within 3D Hydrogel using 3D Bio-Printing Technology. Cell Mol. Bioeng 2014, 7, (3), 460–472. [PubMed: 25484989]
20. Colosi C; Shin SR; Manoharan V; Massa S; Costantini M; Barbetta A; Dokmeci MR; Dentini M; Khademhosseini A, Microfluidic Bioprinting of Heterogeneous 3D Tissue Constructs Using Low-Viscosity Bioink. Adv. Mater 2016, 28, (4), 677–84. [PubMed: 26606883]
21. Jia W; Gungor-Ozkerim PS; Zhang YS; Yue K; Zhu K; Liu W; Pi Q; Byambaa B; Dokmeci MR; Shin SR; Khademhosseini A, Direct 3D bioprinting of perfusable vascular constructs using a blend bioink. Biomaterials 2016, 106, 58–68. [PubMed: 27552316]
22. Choi YJ; Jun YJ; Kim DY; Yi HG; Chae SH; Kang J; Lee J; Gao G; Kong JS; Jang J; Chung WK; Rhie JW; Cho DW, A 3D cell printed muscle construct with tissue-derived bioink for the treatment of volumetric muscle loss. Biomaterials 2019, 206, 160–169. [PubMed: 30939408]
23. Pereira RF; Sousa A; Barrias CC; Bártolo PJ; Granja PL, A single-component hydrogel bioink for bioprinting of bioengineered 3D constructs for dermal tissue engineering. Mater. Horiz 2018, 5, (6), 1100–1111.
24. Rosales AM; Anseth KS, The design of reversible hydrogels to capture extracellular matrix dynamics. Nat. Rev. Mat 2016, 1, (2), 1–15.
25. Jia J; Jeon EJ; Li M; Richards DJ; Lee S; Jung Y; Barrs RW; Coyle R; Li X; Chou JC; Yost MJ; Gerecht S; Cho S-W; Mei Y, Evolutionarily conserved sequence motif analysis guides development of chemically defined hydrogels for therapeutic vascularization. Sci. Adv 2020, 6, (28), eaaz5894. [PubMed: 32923589]
26. Aisenbrey EA; Murphy WL, Synthetic alternatives to Matrigel. Nat. Rev. Mater 2020, 5, (7), 539–551. [PubMed: 32953138]
27. Unal AZ; West JL, Synthetic ECM: Bioactive Synthetic Hydrogels for 3D Tissue Engineering. Bioconjug. Chem 2020, 31, (10), 2253–2271. [PubMed: 32786365]
28. Nicolas J; Magli S; Rabbachin L; Sampaolesi S; Nicotra F; Russo L, 3D Extracellular Matrix Mimics: Fundamental Concepts and Role of Materials Chemistry to Influence Stem Cell Fate. Biomacromolecules 2020, 21, (6), 1968–1994. [PubMed: 32227919]

29. Teixeira SP; Domingues RM; Shevchuk M; Gomes ME; Peppas NA; Reis RL, Biomaterials for sequestration of growth factors and modulation of cell behavior. Adv. Funct. Mater 2020, 30, 1909011.
30. Lavrador P; Gaspar VM; Mano JF, Mechanochemical Patternable ECM-Mimetic Hydrogels for Programmed Cell Orientation. Adv. Healthc. Mater 2020, 9, (10), 1901860.
31. Rowley JA; Madlambayan G; Mooney DJ, Alginate hydrogels as synthetic extracellular matrix materials. Biomaterials 1999, 20, (1), 45–53. [PubMed: 9916770]
32. Axpe E; Oyen ML, Applications of Alginate-Based Bioinks in 3D Bioprinting. Int. J. Mol. Sci 2016, 17, (12), 1976.
33. Massia SP; Hubbell JA, Covalent surface immobilization of Arg-Gly-Asp- and Tyr-Ile-Gly-Ser-Arg-containing peptides to obtain well-defined cell-adhesive substrates. Anal. Biochem 1990, 187, (2), 292–301. [PubMed: 2382830]
34. Bouhadir KH; Lee KY; Alsberg E; Damm KL; Anderson KW; Mooney DJ, Degradation of partially oxidized alginate and its potential application for tissue engineering. Biotechnol. Prog 2001, 17, (5), 945–50. [PubMed: 11587588]
35. Augst AD; Kong HJ; Mooney DJ, Alginate hydrogels as biomaterials. Macromol. Biosci 2006, 6, (8), 623–33. [PubMed: 16881042]
36. Zhang D; Kilian KA, Peptide microarrays for the discovery of bioactive surfaces that guide cellular processes: a single step azide–alkyne “click” chemistry approach. J. Mater. Chem. B 2014, 2, (27), 4280–4288. [PubMed: 32261566]
37. Santana BP; Nedel F; Perelló Ferrúa C; Marques e Silva R; da Silva AF; Demarco FF; Lenin Villarreal Carreño N, Comparing different methods to fix and to dehydrate cells on alginate hydrogel scaffolds using scanning electron microscopy. Microsc. Res. Tech 2015, 78, (7), 553–61. [PubMed: 25871651]
38. Schneider CA; Rasband WS; Eliceiri KW, NIH Image to ImageJ: 25 years of image analysis. Nat. Methods 2012, 9, (7), 671–675. [PubMed: 22930834]
39. Hotaling NA; Bharti K; Kriel H; Simon CG Jr., DiameterJ: A validated open source nanofiber diameter measurement tool. Biomaterials 2015, 61, 327–338. [PubMed: 26043061]
40. Nock R; Nielsen F, Statistical Region Merging. IEEE Trans. Pattern Anal. Mach. Intell 2004, 26, (11), 1452–1458. [PubMed: 15521493]
41. Zudaire E; Gambardella L; Kurcz C; Vermeren S, A Computational Tool for Quantitative Analysis of Vascular Networks. PLoS One 2011, 6, (11), e27385. [PubMed: 22110636]
42. Jia J; Richards DJ; Pollard S; Tan Y; Rodriguez J; Visconti RP; Trusk TC; Yost MJ; Yao H; Markwald RR; Mei Y, Engineering alginate as bioink for bioprinting. Acta Biomater. 2014, 10, (10), 4323–31. [PubMed: 24998183]
43. Brooks PC; Clark RA; Cheresh DA, Requirement of vascular integrin alpha v beta 3 for angiogenesis. Science 1994, 264, (5158), 569–71. [PubMed: 7512751]
44. Wang L; Zhao M; Li S; Erasquin UJ; Wang H; Ren L; Chen C; Wang Y; Cai C, “Click” immobilization of a VEGF-mimetic peptide on decellularized endothelial extracellular matrix to enhance angiogenesis. ACS Appl. Mater. Interfaces 2014, 6, (11), 8401–6. [PubMed: 24749832]
45. Van Hove AH; Antonienko E; Burke K; Brown E 3rd; Benoit DS, Temporally tunable, enzymatically responsive delivery of proangiogenic peptides from poly(ethylene glycol) hydrogels. Adv. Healthc. Mater 2015, 4, (13), 2002–11. [PubMed: 26149620]
46. Su J; Satchell SC; Wertheim JA; Shah RN, Poly(ethylene glycol)-crosslinked gelatin hydrogel substrates with conjugated bioactive peptides influence endothelial cell behavior. Biomaterials 2019, 201, 99–112. [PubMed: 30807988]
47. Leslie-Barbick JE; Saik JE; Gould DJ; Dickinson ME; West JL, The promotion of microvasculature formation in poly(ethylene glycol) diacrylate hydrogels by an immobilized VEGF-mimetic peptide. Biomaterials 2011, 32, (25), 5782–9. [PubMed: 21612821]
48. Ziaco B; Diana D; Capasso D; Palumbo R; Celentano V; Di Stasi R; Fattorusso R; D’Andrea LD, C-terminal truncation of Vascular Endothelial Growth Factor mimetic helical peptide preserves structural and receptor binding properties. Biochem. Biophys. Res. Commun 2012, 424, (2), 290–4. [PubMed: 22749999]

49. D'Andrea LD; Iaccarino G; Fattorusso R; Sorriento D; Carannante C; Capasso D; Trimarco B; Pedone C, Targeting angiogenesis: structural characterization and biological properties of a de novo engineered VEGF mimicking peptide. Proc. Natl. Acad. Sci. USA 2005, 102, (40), 14215–20. [PubMed: 16186493]
50. Santulli G; Ciccarelli M; Palumbo G; Campanile A; Galasso G; Ziaco B; Altobelli GG; Cimini V; Piscione F; D'Andrea LD; Pedone C; Trimarco B; Iaccarino G, In vivo properties of the proangiogenic peptide QK. J Transl. Med 2009, 7, 41. [PubMed: 19505323]
51. Finetti F; Basile A; Capasso D; Di Gaetano S; Di Stasi R; Pascale M; Turco CM; Ziche M; Morbidelli L; D'Andrea LD, Functional and pharmacological characterization of a VEGF mimetic peptide on reparative angiogenesis. Biochem. Pharmacol 2012, 84, (3), 303–11. [PubMed: 22554565]
52. Di Stasi R; Diana D; Capasso D; Di Gaetano S; De Rosa L; Celentano V; Isernia C; Fattorusso R; D'Andrea LD, VEGFR Recognition Interface of a Proangiogenic VEGF-Mimetic Peptide Determined In Vitro and in the Presence of Endothelial Cells by NMR Spectroscopy. Chemistry 2018, 24, (44), 11461–11466. [PubMed: 29799174]
53. Lee S; Jilani SM; Nikolova GV; Carpizo D; Iruela-Arispe ML, Processing of VEGF-A by matrix metalloproteinases regulates bioavailability and vascular patterning in tumors. J. Cell Biol 2005, 169, (4), 681–91. [PubMed: 15911882]
54. Mott JD; Werb Z, Regulation of matrix biology by matrix metalloproteinases. Curr. Opin. Cell Biol 2004, 16, (5), 558–64. [PubMed: 15363807]
55. Martino MM; Tortelli F; Mochizuki M; Traub S; Ben-David D; Kuhn GA; Müller R; Livne E; Eming SA; Hubbell JA, Engineering the growth factor microenvironment with fibronectin domains to promote wound and bone tissue healing. Sci. Transl. Med 2011, 3, (100), 100ra89–100ra89.
56. Cai L; Dinh CB; Heilshorn SC, One-pot Synthesis of Elastin-like Polypeptide Hydrogels with Grafted VEGF-Mimetic Peptides. Biomater. Sci 2014, 2, (5), 757–765. [PubMed: 24729868]
57. Moulisova V; Gonzalez-Garcia C; Cantini M; Rodrigo-Navarro A; Weaver J; Costell M; Sabater ISR; Dalby MJ; Garcia AJ; Salmeron-Sanchez M, Engineered microenvironments for synergistic VEGF - Integrin signalling during vascularization. Biomaterials 2017, 126, 61–74. [PubMed: 28279265]
58. Davis GE; Camarillo CW, Regulation of endothelial cell morphogenesis by integrins, mechanical forces, and matrix guidance pathways. Exp. Cell. Res 1995, 216, (1), 113–23. [PubMed: 7813611]
59. Davis GE; Senger DR, Endothelial extracellular matrix: biosynthesis, remodeling, and functions during vascular morphogenesis and neovessel stabilization. Circ. Res 2005, 97, (11), 1093–107. [PubMed: 16306453]
60. Masson-Gadais B; Houle F; Laferriere J; Huot J, Integrin alphavbeta3, requirement for VEGFR2-mediated activation of SAPK2/p38 and for Hsp90-dependent phosphorylation of focal adhesion kinase in endothelial cells activated by VEGF. Cell Stress Chaperones 2003, 8, (1), 37–52. [PubMed: 12820653]
61. Mahabeleshwar GH; Feng W; Reddy K; Plow EF; Byzova TV, Mechanisms of integrin-vascular endothelial growth factor receptor cross-activation in angiogenesis. Circ. Res 2007, 101, (6), 570–80. [PubMed: 17641225]
62. Somanath PR; Malinin NL; Byzova TV, Cooperation between integrin alphavbeta3 and VEGFR2 in angiogenesis. Angiogenesis 2009, 12, (2), 177–85. [PubMed: 19267251]
63. Ferrara N, The role of VEGF in the regulation of physiological and pathological angiogenesis In Mechanisms of Angiogenesis, Clauss M; Breier G, Eds. Birkhäuser Basel: Basel, 2005; pp 209–231.
64. Rohringer S; Hofbauer P; Schneider KH; Husa AM; Feichtinger G; Peterbauer-Scherb A; Redl H; Holnthoner W, Mechanisms of vasculogenesis in 3D fibrin matrices mediated by the interaction of adipose-derived stem cells and endothelial cells. Angiogenesis 2014, 17, (4), 921–33. [PubMed: 25086616]
65. Traktuev DO; Prater DN; Merfeld-Clauss S; Sanjeevaiah AR; Saadatzadeh MR; Murphy M; Johnstone BH; Ingram DA; March KL, Robust functional vascular network formation in vivo by cooperation of adipose progenitor and endothelial cells. Circ. Res 2009, 104, (12), 1410–20. [PubMed: 19443841]

66. Potter RF; Groom AC, Capillary diameter and geometry in cardiac and skeletal muscle studied by means of corrosion casts. Microvasc. Res 1983, 25, (1), 68–84. [PubMed: 6835100]

67. Hanjaya-Putra D; Bose V; Shen YI; Yee J; Khetan S; Fox-Talbot K; Steenbergen C; Burdick JA; Gerecht S, Controlled activation of morphogenesis to generate a functional human microvasculature in a synthetic matrix. Blood 2011, 118, (3), 804–15. [PubMed: 21527523]

68. Zhao Y; Li Y; Mao S; Sun W; Yao R, The influence of printing parameters on cell survival rate and printability in microextrusion-based 3D cell printing technology. Biofabrication 2015, 7, (4), 045002. [PubMed: 26523399]

69. Paxton N; Smolan W; Bock T; Melchels F; Groll J; Jungst T, Proposal to assess printability of bioinks for extrusion-based bioprinting and evaluation of rheological properties governing bioprintability. Biofabrication 2017, 9, (4), 044107. [PubMed: 28930091]

70. Dubbin K; Tabet A; Heilshorn SC, Quantitative criteria to benchmark new and existing bio-inks for cell compatibility. Biofabrication 2017, 9, (4), 044102. [PubMed: 28812982]

71. Diamantides N; Wang L; Pruiksma T; Siemiatkoski J; Dugopolski C; Shortkroff S; Kennedy S; Bonassar LJ, Correlating rheological properties and printability of collagen bioinks: the effects of riboflavin photocrosslinking and pH. Biofabrication 2017, 9, (3), 034102. [PubMed: 28677597]

72. Gao T; Gillispie GJ; Copus JS; Pr AK; Seol YJ; Atala A; Yoo JJ; Lee SJ, Optimization of gelatin-alginate composite bioink printability using rheological parameters: a systematic approach. Biofabrication 2018, 10, (3), 034106. [PubMed: 29923501]

73. Jungst T; Smolan W; Schacht K; Scheibel T; Groll J, Strategies and Molecular Design Criteria for 3D Printable Hydrogels. Chem. Rev 2016, 116, (3), 1496–539. [PubMed: 26492834]

74. Schwab A; Levato R; D'Este M; Piluso S; Eglin D; Malda J, Printability and Shape Fidelity of Bioinks in 3D Bioprinting. Chem. Rev 2020, 120, (19), 11028–11055. [PubMed: 32856892]

75. Lee SC; Gillispie G; Prim P; Lee SJ, Physical and Chemical Factors Influencing the Printability of Hydrogel-based Extrusion Bioinks. Chem. Rev 2020, 120, (19), 10834–10886. [PubMed: 32815369]

76. Sarker MA; Chen X, Modeling the Flow Behavior and Flow Rate of Medium Viscosity Alginate for Scaffold Fabrication With a Three-Dimensional Bioplotter. J Manuf. Sci. Eng 2017, 139, (8), 081002.

77. Cross MM, Rheology of non-Newtonian fluids: a new flow equation for pseudoplastic systems. J. Colloid Interface Sci 1965, 20, (5), 417–437.

78. Tabriz AG; Hermida MA; Leslie NR; Shu W, Three-dimensional bioprinting of complex cell laden alginate hydrogel structures. Biofabrication 2015, 7, (4), 045012. [PubMed: 26689257]

79. Lee KY; Mooney DJ, Alginate: properties and biomedical applications. Prog. Polym. Sci 2012, 37, (1), 106–126. [PubMed: 22125349]

80. Guvendiren M; Lu HD; Burdick JA, Shear-thinning hydrogels for biomedical applications. Soft Matter 2012, 8, (2), 260–272.

81. Scadden DT, Rethinking stroma: lessons from the blood. Cell Stem Cell 2012, 10, (6), 648–649. [PubMed: 22704500]

82. Barros da Silva P; Coelho M; Bidarra SJ; Neves SC; Barrias CC, Reshaping in vitro Models of Breast Tissue: Integration of Stromal and Parenchymal Compartments in 3D Printed Hydrogels. Front. Bioeng. Biotech 2020, 8, 494.

83. Stunova A; Vistejnova L, Dermal fibroblasts-A heterogeneous population with regulatory function in wound healing. Cytokine Growth Factor Rev. 2018, 39, 137–150. [PubMed: 29395658]

84. Mendez JJ; Ghaedi M; Sivarapatna A; Dimitrievska S; Shao Z; Osuji CO; Steinbacher DM; Leffell DJ; Niklason LE, Mesenchymal stromal cells form vascular tubes when placed in fibrin sealant and accelerate wound healing in vivo. Biomaterials 2015, 40, 61–71. [PubMed: 25433608]

85. Sun Y; Chen S; Zhang X; Pei M, Significance of Cellular Cross-Talk in Stromal Vascular Fraction of Adipose Tissue in Neovascularization. Arterioscler. Thromb. Vasc. Biol 2019, 39, (6), 1034–1044. [PubMed: 31018663]

86. Hielscher A; Ellis K; Qiu C; Porterfield J; Gerecht S, Fibronectin Deposition Participates in Extracellular Matrix Assembly and Vascular Morphogenesis. PLoS One 2016, 11, (1), e0147600. [PubMed: 26811931]

87. Hynes RO, Cell-matrix adhesion in vascular development. J. Thromb. Haemost 2007, 5 Suppl 1, 32–40. [PubMed: 17635706]

88. Massa S; Sakr MA; Seo J; Bandaru P; Arneri A; Bersini S; Zare-Eelanjegh E; Jalilian E; Cha BH; Antona S; Enrico A; Gao Y; Hassan S; Acevedo JP; Dokmeci MR; Zhang YS; Khademhosseini A; Shin SR, Bioprinted 3D vascularized tissue model for drug toxicity analysis. Biomicrofluidics 2017, 11, (4), 044109. [PubMed: 28852429]

89. Potjewyd G; Moxon S; Wang T; Domingos M; Hooper NM, Tissue Engineering 3D Neurovascular Units: A Biomaterials and Bioprinting Perspective. Trends Biotechnol. 2018, 36, (4), 457–472. [PubMed: 29422410]

90. Hinton TJ; Jallerat Q; Palchesko RN; Park JH; Grodzicki MS; Shue HJ; Ramadan MH; Hudson AR; Feinberg AW, Three-dimensional printing of complex biological structures by freeform reversible embedding of suspended hydrogels. Sci. Adv 2015, 1, (9), e1500758. [PubMed: 26601312]

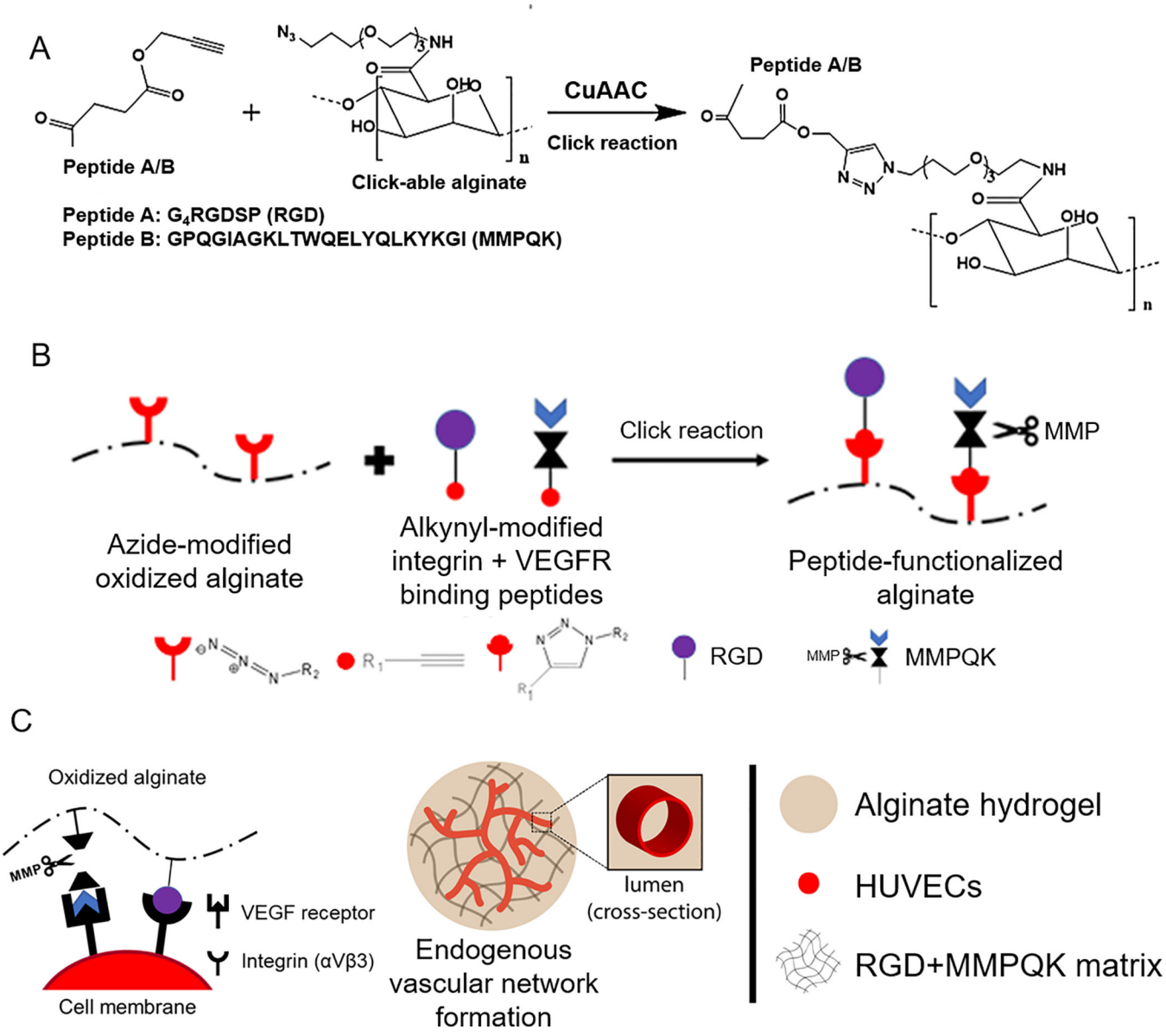

Figure 1.

Vasculogenic hydrogel matrix design. (A) Chemical schematic of functionalized alginate synthesis via CuAAC chemistry. (B) Schematic illustration of functionalized alginate synthesis with click-able integrin-binding and protease-sensitive VEGF receptor binding peptides. (C) Schematic illustration of cell-matrix interactions and endogenous vascularization within the alginate matrix.

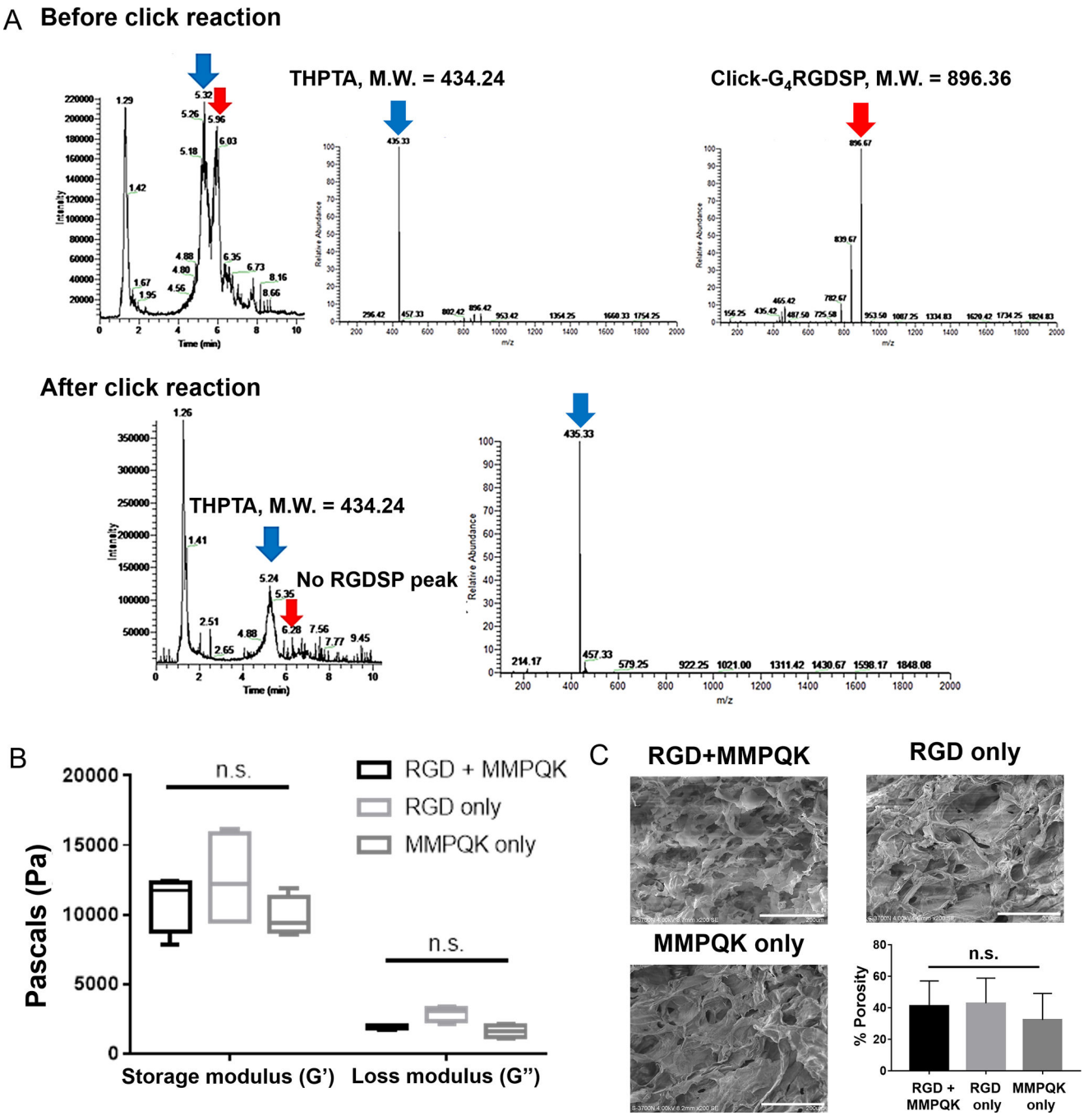

Figure 2.

Characterization of peptide-functionalized alginate hydrogels. (A) LC and MS spectrum of RGDSP peptide and CuAAC catalytic complex before and after Click conjugation to alginate. Blue arrow indicates the corresponding peaks of THPTA (M.W.=434.25 kDa, copper coordinating compound). Red arrow indicates the corresponding peaks of RGDSP peptide (M.W.=896.36 kDa). (B) Storage and loss modulus of peptide-functionalized (2% w/v) alginates measured by oscillatory frequency sweep from 0.1 to 10 Hz at 1% strain; n≥4 for each group; n.s. no significant difference. (C) Representative SEM images of peptide-

functionalized alginate hydrogel microstructures and quantification of scaffold percent porosity. Scale bars = 200 μm.

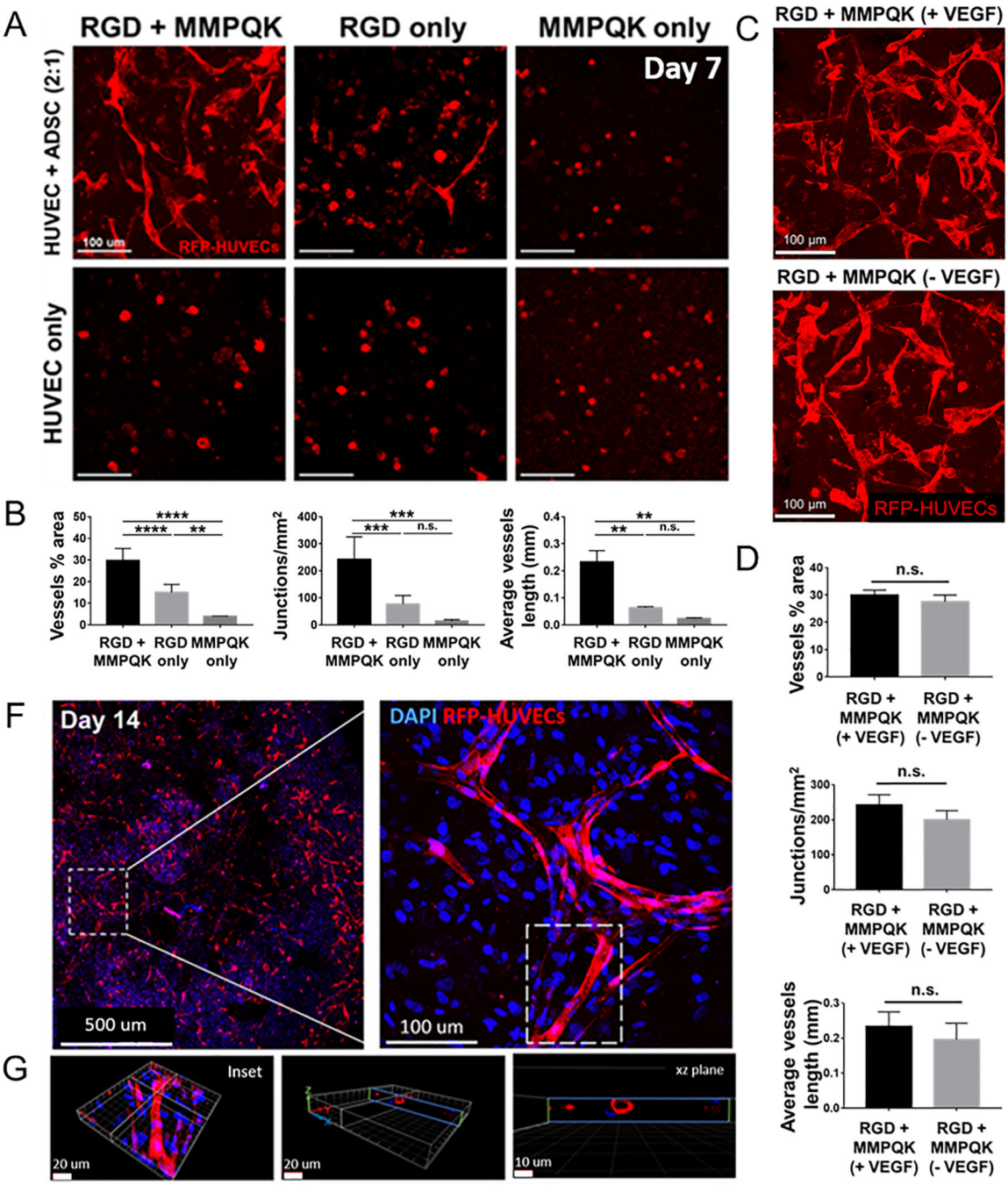

Figure 3.

Vascular morphogenesis in peptide-functionalized alginate hydrogels. (A) Representative day 7 images of RFP-HUVECs cultured with or without ADSCs in 2% (w/v) peptide-functionalized alginates. (B) The quantification of vascular morphogenesis at day 7, n≥4 for each group (* $p < 0.05$, ** $p < 0.01$, n.s. not significant). (C) Representative day 7 images of microvascular networks in RGD+MMPQK hydrogels (2:1 HUVEC:ADSC coculture) with or without VEGF in the culture media. (D) Quantification of vascular morphogenesis with or without VEGF, n≥4 for each group. (E) Microvascularization at day 14 in 2% (w/v) alginates

functionalized with RGD and MMPQK. (F) 3D reconstruction and ortho-slices showing a lumenized (*) endothelial tube.

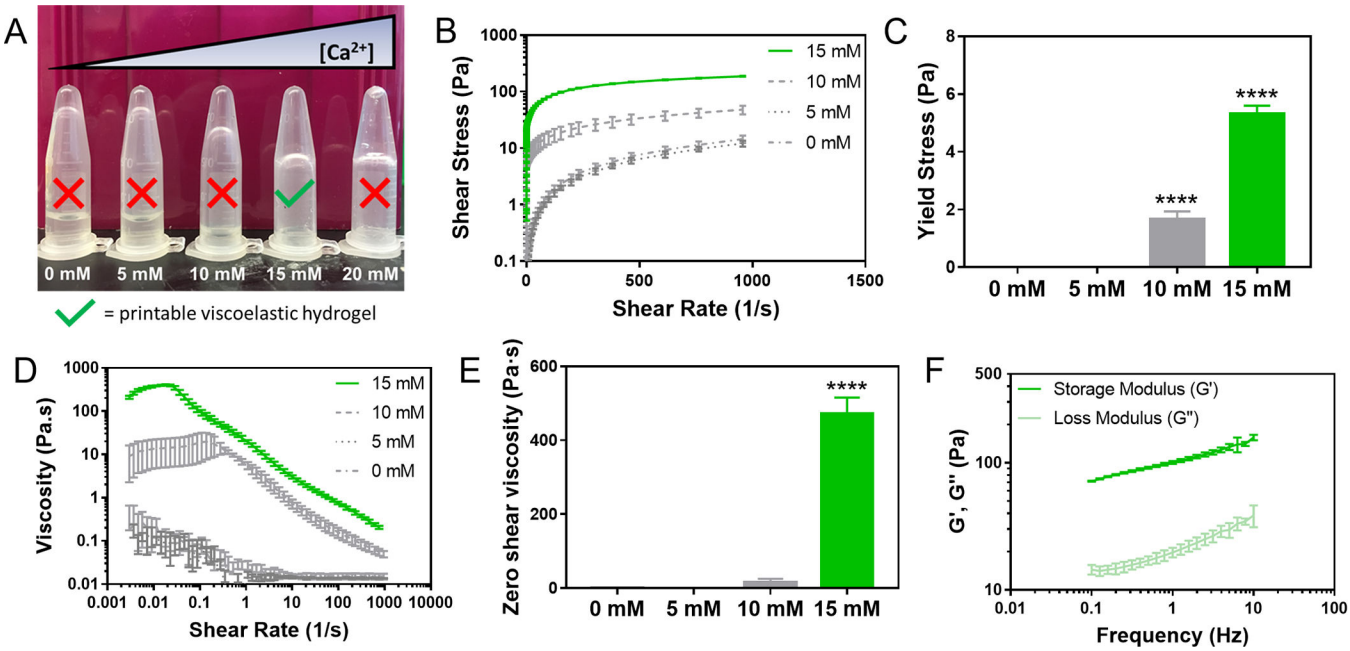

Figure 4.

Tuning the rheological properties of alginate hydrogel precursors via partial ionic crosslinking. (A) Increasing concentrations of $CaCl_2$ (0–20 mM) were added to 2% (w/v) alginate hydrogel precursors to yield progressively crosslinked solutions. (B) Flow curves for shear stress as a function of shear rate for partially crosslinked alginate solutions, n≥3 for each group. (C) Yield stress measurements of the partially crosslinked alginate solutions as determined using the Herschel-Bulkley model. (D) Flow curves for viscosity as a function of shear rate for partially crosslinked alginate solutions, n≥3 for each group. (E) Zero shear viscosity measurements of the partially crosslinked alginate solutions as determined using the Cross model. (F) Oscillatory rheological behavior of 15 mM solution, n≥3 for each group (**** $p < 0.0001$, significant difference from all groups).

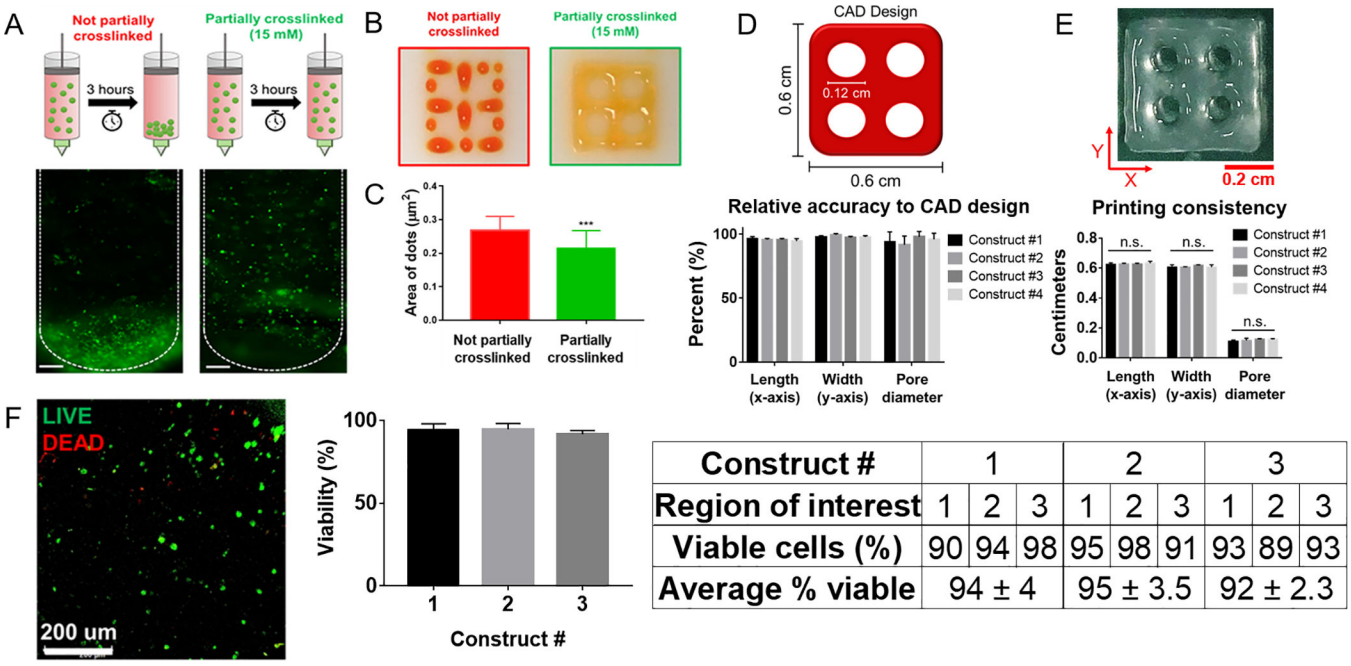

Construct #	1			2			3		
Region of interest	1	2	3	1	2	3	1	2	3
Viable cells (%)	90	94	98	95	98	91	93	89	93
Average % viable	94 ± 4			95 ± 3.5			92 ± 2.3		

Figure 5.

Printability of the partially crosslinked RGD+MMPQK alginate bioink. (A) Cell sedimentation test in 2% (w/v) alginates that were or were not partially crosslinked with 15 mM $CaCl_2$. Scale bar = 200 micrometers. (B) Lattice constructs printed with functionalized alginate bioink using a point-to-point fabrication method with or without partial crosslinking. (C) Resolution of printed hydrogel dots, n = 25 for each group (*** $p<0.001$). (D) Relative print accuracy of construct dimensions compared to the original dimensions of the CAD design. (E) Representative image of a printed construct and quantification of print consistency in four consecutively printed lattices. n.s. not significant. (F) Live/Dead assay immediately post-print and quantification of live cells in printed constructs. Cell viability in three regions of interest (ROIs) in each of three printed constructs was evaluated.

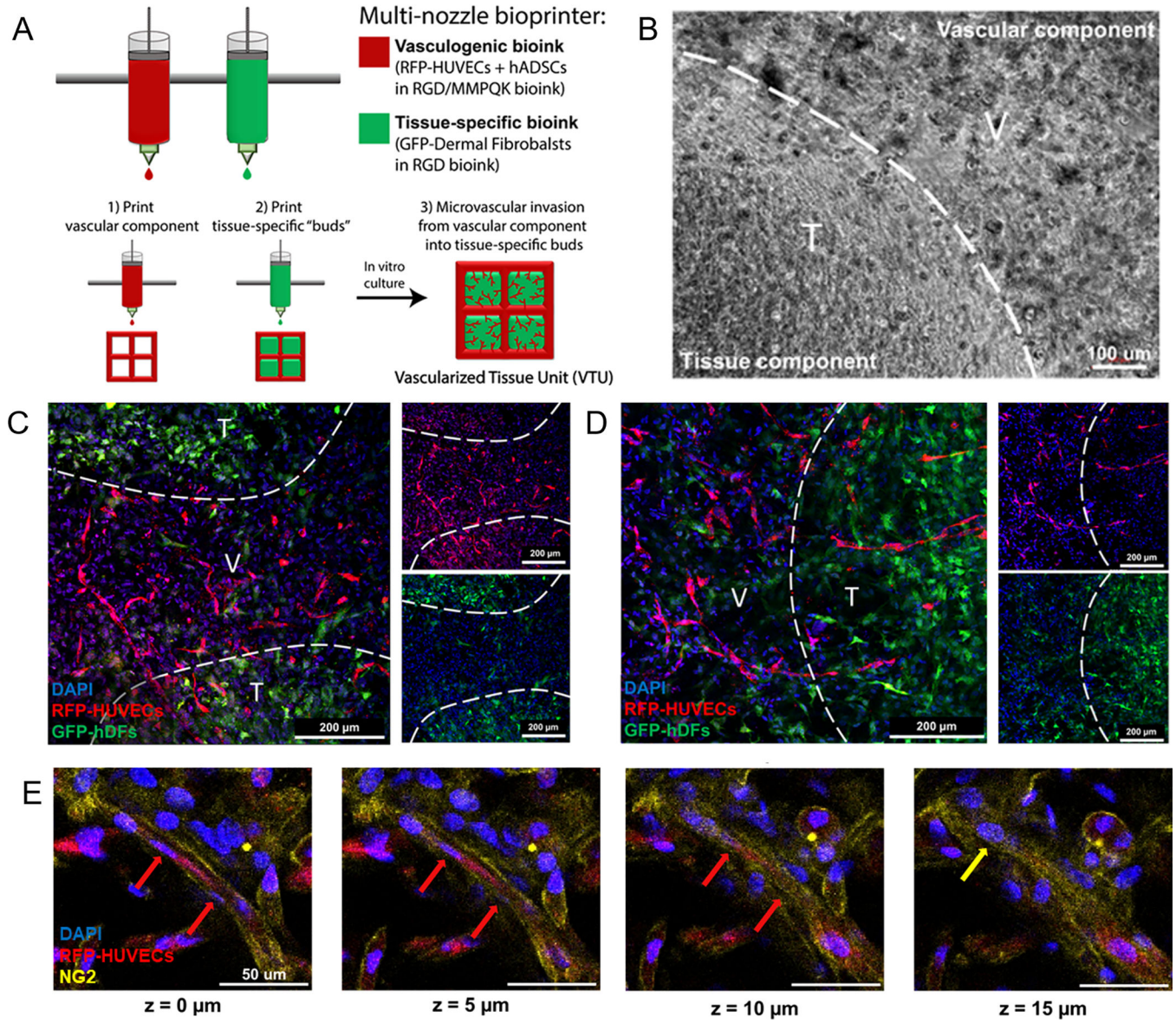

Figure 6.

Fabricating a vascularized Tissue Unit (VTU) with partially crosslinked RGD+MMPQK alginate bioink. (A) Conceptual design of the Vascularized Tissue Unit (VTU). (B) Brightfield image of a bioprinted VTU (V, vascular components; T, tissue components). Scale bars = 100 μm. (C) Representative images of edge region of the VTU at day 7: V, vascular components; T, tissue components. Scale bars = 200 micrometers. (D) Representative images of middle region of the VTU at day 7. Scale bars = 200 micrometers. (E) Slices from a confocal z-stack show RFP-HUVECs colocalized with NG2+ cells in the printed VTU after 7 days. At z=0 um, the nuclei of RFP-HUVECs (red arrows) can be seen. At z=5 um and z=10 um, the nuclei are obscured by NG2+ cells, and the nuclei of NG2+ cells can be seen with clarity at z=15 um (yellow arrow). Scale bars = 50 micrometers.

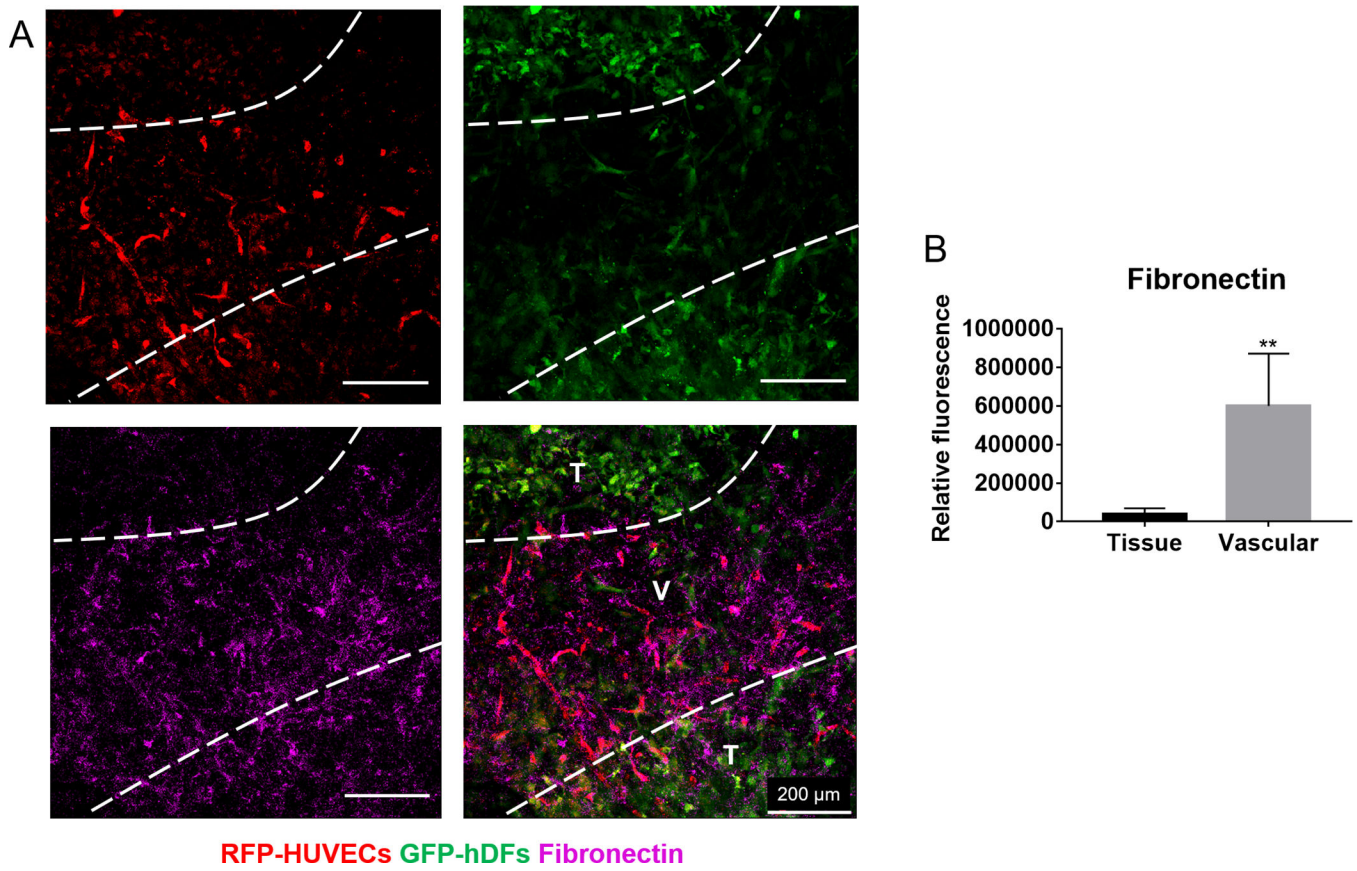

Figure 7.

ECM deposition in the vascular component of the printed VTU. (A) Fibronectin deposition in the printed VTU after 7 days. (B) Relative fluorescence of fibronectin in vascular and tissue components (** $p < 0.01$). Scale bars = 200 micrometers.